AIChE WILEY InterScience DISCOVER SOMETHING GREAT

ENVIRONMENTAL AND ENERGY ENGINEERING

Multiscale Modeling and Optimization of H_2 Storage Using Nanoporous Adsorbents

Eustathios S. Kikkinides and Maria Konstantakou
Dept. of Engineering and Management of Energy Resources, University of Western Macedonia, 50100 Kozani, Greece

Michael C. Georgiadis
Dept. of Chemical Engineering, Centre for Process Systems Engineering, Imperial College London, London SW7 2AZ, U.K.

Theodore A. Steriotis and Athanasios K. Stubos
National Center for Scientific Research "Demokritos," Institute of Nuclear Technology and Radiation Protection, Athens, Greece

DOI 10.1002/aic.10910
Published online June 5, 2006 in Wiley InterScience (www.interscience.wiley.com).

The aim of the present study is the development of a multiscale modeling and optimization framework for hydrogen storage in carbon-based nanoporous adsorbents. The outlined methodology is generic and can be easily adapted to the storage of several gases of relevant importance and/or different physisorbing nanoporous materials. The results indicate clearly how operating constraints (such as temperature limitations arising from safety considerations) can affect the material design in terms of its pore size distribution and how material design constraints (such as those arising from manufacturing limitations) can effect the operation and efficiency of the process. The ultimate objective is to systematically reveal the strong and highly related synergistic benefits between process design/operation decisions and material design aspects so as to ensure an economically attractive, technically feasible, and safe process. © 2006 American Institute of Chemical Engineers *AIChE J,* 52: 2964–2977, 2006
Keywords: multiscale modeling, adsorption/gas, optimization, hydrogen storage.

Introduction

Environmental and energy problems related to the emission of greenhouse gases and to the depletion of fossil-fuel natural resources have led to significant efforts to investigate alternative and cleaner fuels.[1] During the coming century, gasoline is expected to be replaced by a cleaner, renewable motor fuel such as hydrogen, whereas fuel cells should take the place of the internal combustion engine. An excellent review discussing the key barriers related to the production of inexpensive hydrogen is given by Agrawal et al.[2] One of the main barriers toward widespread usage of hydrogen energy in the automotive industry is the storage problem. Conventional storage methods such as gas compression and liquefaction are impractical because the former requires either excessively large tank volumes or extremely high pressures and the latter is too expensive to be used in public vehicles.[3] Storing hydrogen in advanced solid materials, such as carbon-based porous adsorbents and metal hydrides, appears to be a promising, cost effective, and safe method of hydrogen storage in the near future. The operation of

E. S. Kikkinides is also affiliated with the Chemical Process Engineering Research Institute, Centre for Research and Technology Hellas, P.O. Box 361, GR 570 01 Thermi, Thessaloniki, Greece.
M. Konstantakou is also affiliated with National Center for Scientific Research "Demokritos," Institute of Nuclear Technology and Radiation Protection, 15310 Ag. Paraskevi Attikis, Athens, Greece.
Correspondence concerning this article should be addressed to E. S. Kikkinides at kikki@uowm.gr.

hydrogen storage tanks packed with these materials presents distinct challenges in process modeling and optimization.[4-8]

Hydrogen storage by adsorption at a relatively low pressure ($\leq$15 MPa) and room temperature offers the advantage of considerably reduced risks in comparison to those associated with the need for very high pressure and additional energy for cooling purposes. To make this method viable, the adsorption capacity of the adsorbent must be such so as to allow storage of a sufficient amount of hydrogen at a relatively short filling time. Temperature limitations may have to be considered during the charging process to take account of potential safety and performance considerations. Lamari et al.[5] studied theoretically and experimentally the thermal effects in dynamic hydrogen storage by adsorption at room temperature and high pressure. A detailed 2-D model describing adsorption-based hydrogen storage was developed by Delahaye et al.[6] Ways to minimize heat effects to maximize the storage capacity were theoretically studied.

From the process perspective most of the literature studies present macroscopic models describing the dynamic behavior of hydrogen storage either in metal hydride beds[4,7,8] or in carbon-based materials.[5,6] On the other hand, detailed simulation studies of hydrogen adsorption in carbon nanotubes or graphitic nanofibers, using molecular simulation methodologies, have also been reported.[9-12] In a recent study,[12] Bhatia and Myers examined thermodynamically the adsorption–desorption cycle of hydrogen and methane in carbon-based porous adsorbents, and have set optimum conditions for adsorptive storage at the material level, based on the total adsorption–desorption cycle. Very little attention has been paid to exploring the synergistic benefits between material design and process operation/design with a view toward deriving a process, which on one hand can operate safely and on the other in the most economically attractive way. These considerations motivate the need for investigating multiscale modeling and optimization strategies.

The concept of *multiscale modeling* is a novel and powerful idea, pervading literature in the field of chemical engineering and suitable for studying complex process systems manifesting phenomena of significant complexity in multiple scales of length and time.[13] Typically, modeling studies addressing design and simulation of chemical engineering processes encompass combinations of at most five standard length scales[14]:

(1) *Nanoscale level*—molecular modeling for ab initio calculation of thermodynamic properties

(2) *Microscale level*—modeling of novel composite materials such as semiconductors, catalysts, adsorbents, as well as polymer and biomolecular systems

(3) *Macroscale level*—process modeling for engineering design of different unit operations

(4) *Kiloscale level*—plantwide simulations for process systems operability and control studies

(5) *Megascale level*—intercontinental production planning/supply chain management studies

The conventional approach of addressing this complexity is to focus on each scale separately, to derive the best possible understanding of relevant phenomena by individual descriptions, extracting phenomenological equations that can then be incorporated in mathematical models. Couplings and interactions between different scales are handled by aggregate descriptions of physical behavior at each scale, subsequently used in modeling the behavior at higher scales. An important characteristic is the absence of computational integration of these descriptions, which are indirectly interfaced by ad hoc approaches in sequential, asynchronous patterns. This *scale decomposition* approach to process modeling has long been remarkably efficient, enabling design and simulation of numerous conventional unit operations.[14] Nevertheless, modern chemical process applications often reach a point where aggregation limits modeling effectiveness and impedes the use of improved descriptions of the underlying physicochemical phenomena (especially when the latter are not available in analytical form).

In this context, a key issue in the hydrogen storage problem using carbon-based nanoporous materials is the material evaluation and design, which is systematically explored by the simulation of hydrogen storage at a molecular level to predict the hydrogen sorption capacity of the selected material. Furthermore, economic and operability considerations motivate the need for a maximum storage capacity while ensuring satisfaction of certain operating constraints. For example, large temperature differences in the process have detrimental effects on the storage performance and may also lead to material deterioration and potential explosions. On the other hand, realistic charging times are required (of the order of several minutes) to have an economically and practically viable storage process.

The present work presents an integrated approach that formally exploits the benefits between material and process design. Systematic simulation and optimization studies are performed at two different length scales: adsorbent pore level and storage tank level. A detailed 2-D mathematical model is developed, describing the hydrogen storage in the bed using carbon-based material. Heat, mass, and momentum transfer effects are modeled in detail. The model is implemented in the gPROMS ™ [Process Systems Enterprise Ltd. (www.psenterprise.com)] modeling environment. A dynamic optimization approach determines the optimal values of the macroscopic sorption parameters taking into account several realistic constraints while ensuring maximum storage efficiency. Then, molecular simulation techniques are used to determine the pore size distribution of the adsorbents, taking into account the optimal macroscopic sorption properties of the material. The whole procedure is iterative because of the interdependence of the heat of adsorption and the bulk density of the adsorbent, used in the macroscopic model, with the optimal pore size distribution obtained from the microscopic model. The effect of realistic process constraints on the material design is illustrated. Limitations reflecting potential manufacturing constraints on specific pore size distributions are taken into account and their effect on the process efficiency and operation is systematically revealed.

Formulation of the Physical Problem

The storage of hydrogen in tanks filled with adsorbents is a process that involves physicochemical phenomena that occur at different length scales. The different length scales typically involved in the process under question are schematically depicted in Figure 1. Consider a cylindrical tank filled with a carbon-based adsorbent. Such a unit typically has a length of the order of 0.25–0.5 m and a diameter of 0.1–0.2 m. On the

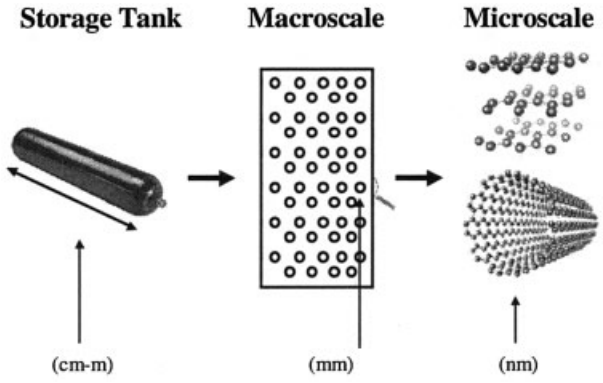

Figure 1. Graphical representation of the multiscale modeling concept in this work.

other hand, the adsorbent material used to fill the tank is in the form of particles with size of the order of 0.5–2 mm. Each particle has an inner pore space the description of which is complicated by the existence of a distribution of pore sizes and shapes. Nanoporous carbons have been successfully represented in the past as pore networks consisting of pores of idealized geometry in the form of slits or cylinders. Detailed characterization studies on these materials have revealed pore size distributions from 0.6 to 2–3 nm. In the present study we have considered slit-shape geometry corresponding to graphitic structures and sizes ranging from 0.6 to 2 nm. It has been shown elsewhere[10] that considering pores with sizes > 2 nm will not increase the excess adsorption and thus the amount of hydrogen adsorbed in the pore. The above pore model is considered to be an appropriate first-order approximation to graphitic nanostructures.

Microscopic Simulation of Hydrogen Storage in Carbon-Based Materials

Monte Carlo–based molecular simulation methods have been extensively used to determine the amount of hydrogen adsorbed (physisorbed) in specific porous materials. In the Grand Canonical Monte Carlo (GCMC) method, the chemical potential (or gas fugacity), volume, and temperature of the system are fixed and the simulation calculates the number of particles (gas molecules) in the system and the configurational energy corresponding to a particular choice of n, V, and T. The method is discussed in detail in a number of books.[15,16] In the present study, the system is considered to be a classical one (that is, the quantum mechanical character of hydrogen is ignored, as shown below). This is likely to be a tolerable approximation at ambient temperatures if the fluid is not particularly dense.[11]

Molecular interactions

Hydrogen–hydrogen interactions were modeled using Lennard–Jones potential

$$u_{HH} = 4\varepsilon_{HH}\left[\left(\frac{\sigma_{HH}}{r}\right)^6 - \left(\frac{\sigma_{HH}}{r}\right)^{12}\right] \quad (1)$$

where u_{HH} is the energy of the (pairwise) interaction between Lennard–Jones sites and ε_{HH} and σ_{HH} are the well depth energy and hard-sphere diameter parameters for the interaction, respectively. A two-site Lennard–Jones model is used, with the interactions summed over all site–site interactions. The parameters for the two-site model were devised in full accordance with similar recent studies.[11] Other important input parameters to the model are given in Cracknell.[11] The potential was cut off at 2 nm and no long-range correction was applied.

Adsorbent–adsorbate interactions

Pore walls are treated as stacked layers of carbon atoms separated by a distance $\Delta = 0.335$ nm, and having a number density $\rho_w = 114$ atoms/nm^3 per layer. The theoretical surface area of this idealized adsorbent is 2620 m^2/g.[10,11] The slit-pore width (H) is defined as the carbon to carbon distance on opposing pore walls. This may have a number of values depending on the method of preparation of the carbon-based material. Because the simulation uses periodic boundary conditions, the pore is modeled as being infinite in two dimensions. The simulation thus does not model any edge effects. The interaction between hydrogen and each wall of the micropore is given by the "10-4-3" potential of Steele[17]:

$$u_w(z) = 2\pi\rho_w\varepsilon_{CH}\sigma_{CH}^2\Delta\left[\frac{2}{5}\left(\frac{\sigma_{CH}}{z}\right)^{10} - \left(\frac{\sigma_{CH}}{z}\right)^4 - \frac{\sigma_{CH}^4}{3\Delta(0.61\Delta + z)^3}\right] \quad (2)$$

This interaction potential models only dispersion forces between adsorbate and adsorbent (that is, no chemisorption effects are included). The Lennard–Jones parameters for the hydrogen–wall interaction were found from the parameters given in Cracknell,[11] which were then combined with graphite Lennard–Jones parameters ($\sigma_{CC} = 0.340$ nm, $\varepsilon_{CC}/k = 28$ K) using the standard Lorentz–Berthelot rules: $\sigma_{CH} = (1/2)[\sigma_{CC} + \sigma_{HH}]$, $\varepsilon_{CH} = \sqrt{\varepsilon_{CC}\varepsilon_{HH}}$.

In addition to the above, z is the distance between the Lennard–Jones site on the adsorbent and the plane of carbon atoms in the pore wall. It must be noticed that Eq. 2 does not take into account the energetic inhomogeneity of the surface along the x and y directions at a distance z from the wall. Nevertheless, this lack of surface corrugation is not expected to affect the results significantly, especially at ambient temperatures.[18]

The potential energy U_w attributed to the walls inside the slit pore model for each atom of the adsorbate molecules is given by the expression

$$U_w = u_w(z) + u_w(H - z) \quad (3)$$

where H is the carbon to carbon distance. For the determination of pore size distributions the corrected width H' should be used because this is the one involved in the experimentally obtained isotherms, that is,

$$H' = H - 2z_0 + \sigma_{HH} \quad (4)$$

where $z_0 = 0.8506\sigma_{CH}$. The potential field in the pore is calculated by the sum of the interactions between the hydrogen and both pore walls.

Note that in modeling the interactions of the hydrogen molecules we have neglected any quantum effects of H_2. Such effects were found to be significant at very low temperatures of 20–50 K.[9,10,19] At such temperatures, the path-integral formalism should be followed to account for the quantum effects of H_2.[20,21] Accordingly, Wang and Johnson[10,22] adopted the Path Integral Monte Carlo to simulate H_2 adsorption at low temperatures, whereas for temperatures $>$ 70 K, Levesque et al.[19] showed than an effective Feynman–Hibbs potential, which is a correction to the classical Lennard–Jones potential, is sufficient to estimate the quantum effects exactly to the order of h^2, where h is Planck's constant.

Before we leave this section, we would like to comment on the selection of the surface–fluid interaction model in the present study. The "10-4-3 " potential has been routinely used for the simulation of sorption in carbon slit-size nanopores. In fact the GCMC method using the above potential is actually included as a module of modern porosimeter software. However, this potential (integrated over an infinite number of carbon layers) is fundamentally in contradiction with the very existence of a high surface area porous solid made up by pores as it was developed for a free surface. A more correct approach would be to use the "10-4 " Steele potential,[23] or calculate full Lennard–Jones potentials either for single-layered or for two- to three-layered carbon walls. Nevertheless, there are two reasons that support the use of the "10-4-3 " potential in the present study:

(1) The use of alternative potentials as well as the effect of having pores with variable pore thickness have been studied and the results point to the conclusion that, especially for slits, the energy minima of adsorption potentials is indeed a varying function of the pore wall thickness but only up to three to five layers and remains practically unchanged for more than five layers.[23] In practical terms this means that when using the Steele potential one is assuming a minimum wall thickness of four to five layers. One could then calculate that the surface area of such a material falls well within the values calculated or experimentally measured for a large number of porous carbons (500–900 m^2/g). Of course much larger surface areas (sometimes $>$3000 m^2/g) have also been reported in the literature; nevertheless, it should be noted that in many cases the measured values exceed by far the surface area that is calculated for a single graphene sheet ($\sim$2600 m^2/g), and the estimated surface area of an extremely thin two-layered wall is about 1200 m^2/g. This is another traditional inconsistency in porous carbon research but out of the scope of this paper.

(2) The scope of the present work is not the development of a novel theoretical description of the solid–fluid and/or fluid–fluid potentials, neither a new approach on GCMC simulations of adsorption in carbon nanopores. On the contrary, a rather simple, well-known, and moreover well-established methodology is used to reveal a novel methodology and route that can couple macroscopic observations or engineering aspects with the microscopic structural details of a solid. In this respect the essence of the work presented is not directly relevant with the adsorbent–adsorbate potential used. Obviously it might be more nearly correct to use a more elaborate surface–fluid interaction model, although the possible errors induced by such aspects as neglecting surface corrugation and other chemical/structural inhomogeneities (such as the existence of active sites, graphene edges, etc.) are perhaps more severe. On the same framework the use of Ewald-type summations as well as the calculation of quantum contributions to the fluid–fluid and fluid–surface potential would definitely constitute a more robust model. However, we strongly believe that the use of such a model would not change our general approach or our conclusions.

GCMC Simulation Experiments

Adsorption isotherms

The Grand Canonical Ensemble Monte Carlo method was used to probe the statistically important regions of the configuration space in the (μ, V, T) ensemble according to the prescription given elsewhere.[16] For the H_2 linear molecules three types of move are attempted with equal probability:

(1) A compound move enabling random displacement and reorientation, with the maximum allowed displacement being adjusted so that the acceptance ratio of the move is about 20% to sample phase space more efficiently.

(2) A compound move consisting of random insertion of the center of mass of a molecule in a random orientation, by generating a unit vector distributed uniformly on the surface of a sphere centered at the origin of the Cartesian system of coordinates of the simulation box (Marsaglia's algorithm[16]).

(3) A random deletion of a fluid molecule.

Periodic boundary conditions have been applied in the directions other than the width of the slit. The simulations were typically run for 5 million configurations and used up to 800 particles. For a given simulation, the size of the box (that is, the two dimensions other than H) was varied to ensure that sufficient particles ($\sim$500–800) remained in the simulation box at each pressure. Statistics were not collected over the first 3×10^6 configurations to ensure adequate convergence of the simulation. The uncertainty on the computed equilibrium properties such as ensemble averages of the number of adsorbate molecules in the box and the total potential energy is estimated to be $<$4%.

Isosteric heat of adsorption

As noted above, during the simulation runs the mean potential energy $\langle U \rangle$ of the sorbed molecules is also calculated as an ensemble average. This quantity represents an integral energy of sorption arising from adsorbate–adsorbent and adsorbate–adsorbate interaction. A related differential property derived from $\langle U \rangle$ is the isosteric heat of adsorption q_{st}, which is defined as the difference between the molar enthalpy of the adsorbate molecule in the gas phase and its partial molar enthalpy in the adsorbed phase, that is,

$$\langle q_{st} \rangle = (-\Delta H) = H^G - \bar{H}^S \tag{5}$$

At low occupancies, in the Henry's law region, the following equation can be derived:

$$\lim_{d \to 0} \langle U \rangle = -\lim_{d \to 0} q_{st} + k_B T \tag{6}$$

Equation 6 provides a convenient way of calculating isosteric heat at zero coverage per molecule $q_{st}^0 \equiv \lim_{d\to 0} q_{st}$ by evaluating numerically the multidimensional integrals

$$\langle U \rangle = \frac{\int d\mathbf{r} d\boldsymbol{\psi} U(\mathbf{r}, \boldsymbol{\psi}) \exp[-\beta U(\mathbf{r}, \boldsymbol{\psi})]}{\int d\mathbf{r} d\boldsymbol{\psi} \exp[-\beta U(\mathbf{r}, \boldsymbol{\psi})]} \tag{7}$$

To evaluate Eq. 7 we used the method of Monte Carlo integration over the configurational space, by calculating the potential energy experienced by one adsorbate molecule for a statistically sufficient number of vectors of position $\mathbf{r}$ and Eulerian angles $\boldsymbol{\psi}$, randomly generated from a uniform probability distribution function. We also calculated the isosteric heat of adsorption at zero coverage in a different way by evaluating the integrals of Eq. 7 using the method of Metropolis Monte Carlo, that is, by using importance sampling to explore the configurational space. Both techniques gave results in very satisfactory agreement.

Macroscopic Modeling of Hydrogen Storage in the Tank

A two-dimensional pseudohomogeneous macroscopic model is developed based on mass, momentum, and energy balances assuming a cylindrical bed packed with a carbon-based adsorbent.[6,24,25]

Material balance

$$\varepsilon \frac{\partial \rho}{\partial t} + \nabla \cdot (\rho \mathbf{u}) + (1 - \varepsilon) \frac{\partial q}{\partial t} = 0 \tag{8}$$

where ρ is the H_2 density in the gas phase, $\mathbf{u}$ is the superficial velocity vector, and q is the hydrogen concentration in the adsorbed phase (in kilograms of hydrogen adsorbed per cubic meter of carbon-based adsorbent). The porosity ε used in the model is the interparticle porosity of the bed, assuming that there is no compression in the micropores, as was previously considered in Delahaye et al.[6]

Energy balance

$$\frac{d}{dt}\left[\varepsilon \rho C_{pg} T + (1 - \varepsilon)\rho_s C_{ps} T - \varepsilon \frac{\rho RT}{M_{H_2}}\right] + \nabla(\rho C_{pg} \mathbf{u} T - \boldsymbol{\lambda}_e \nabla T) + (1 - \varepsilon)(-\Delta H) \frac{\partial q}{\partial t} = 0 \tag{9}$$

where T is the temperature of the bed, λ_e is the effective thermal conductivity, C_{ps} is the solid heat capacity, ρ_s is the bulk density of the adsorbent, and $(-\Delta H)$ is the heat of adsorption.

Momentum balance

The steady-state momentum balance of laminar gas flow through a packed bed can be expressed by Darcy's law:

$$u_r = -\left(\frac{\mathbf{K}}{\mu}\right) \cdot \nabla P \tag{10}$$

where $\mathbf{K}$ is the permeability tensor of the bed and P is the bed pressure. In many cases the Blake–Cozeny equation, which is the equivalent expression for random sphere packs, is used.[24,25]

Adsorption kinetics

The adsorption kinetics are approximated by the linear driving force (LDF) model[26]:

$$\frac{dq}{dt} = k(q^* - q) \tag{11}$$

where q^* is the adsorbed gas in equilibrium with the gas phase and k is a given parameter potentially expressing a mass transfer coefficient in an aggregated level. In general a more rigorous approach should involve the solution of the diffusion equation at the micro- and/or macropore level. Nevertheless, it has been shown that for sufficiently fast diffusion times t_D, compared to the storage time t_s ($t_s/t_D \geq 0.1$), the LDF model is quite accurate, corresponding to a quadratic concentration profile in the adsorbent particle.[27,28]

Adsorption equilibrium

In general an equilibrium isotherm is used to describe the adsorbate–adsorbent interactions at the macroscopic level. It was shown before that, at ambient temperatures, the adsorption of H_2 in carbon-based materials is well described by the Langmuir isotherm. Thus in the present study a Langmuir-type isotherm is assumed as was also supported by additional molecular simulation experiments.

The Langmuir isotherm is described by the following equation:

$$q^* = \frac{q_s b P}{1 + bP} = \frac{q_s b_0 \exp[-\Delta H/RT] P}{1 + b_0 \exp[-\Delta H/RT] P} \tag{12}$$

where q_s and b_0 are parameters depending on the selected material and P, the total pressure. Parameter $(-\Delta H)$ is the heat of adsorption and in the present study is considered to be identical to the isosteric heat of adsorption obtained from the microscopic model, in accord with the considerations embedded in the Langmuir isotherm. However, in general, ΔH is expected to vary with coverage as a result of energetic and structural heterogeneity effects.[29] Nevertheless, in the present study we have considered that ΔH does not vary significantly with coverage at the macroscopic scale, in accord with previous studies,[5,6] an assumption that has to be confirmed from the results of the microscopic simulation. The optimal values of the material-dependent parameters q_s and b_0 are determined in the present study.

Boundary and initial conditions

The necessary boundary and initial conditions to complement the model equations, are given below.

At the Tank Inlet ($z = 0$) Dirichlet BCs:

$$\rho = \rho_f \tag{13a}$$

$$T = T_f \tag{13b}$$

where ρ_f and T_f are the inlet values of ρ_f and T_f, respectively.

For the case of pressure we have

$$\begin{aligned} P &= P_f \cdot (t/a) \qquad 0 \le t \le t_c \\ P &= P_f \qquad\quad\; t_c \le t \le t_s \end{aligned} \tag{13c}$$

where t_c is the charging time, t_s is the storage time, P_f is the charging pressure at the end of storage, and a is an operating parameter that determines the rate of charging the bed with hydrogen. In the majority of the simulations it was considered that $t_c = t_s$. In such a case it is obvious that $a = t_c$.

At the Tank Outlet ($z = L$)

$$\frac{\partial \rho}{\partial z} = 0 \tag{14a}$$

$$-\lambda_e \frac{\partial T}{\partial z} = h(T - T_c) \tag{14b}$$

$$u_z = u_r = 0 \tag{14c}$$

At the Tank Center ($r = 0$)

$$\frac{\partial \rho}{\partial r} = 0 \tag{15a}$$

$$\frac{\partial T}{\partial r} = 0 \tag{15b}$$

$$\frac{\partial u_z}{\partial r} = \frac{\partial u_r}{\partial r} = 0 \tag{15c}$$

At the Tank Wall ($r = 1$)

$$\frac{\partial \rho}{\partial r} = 0 \tag{16a}$$

$$-\lambda_e \frac{\partial T}{\partial r} = h(T - T_c) \tag{16b}$$

$$u_z = u_r = 0 \tag{16c}$$

Note that in the present model we have used an overall heat transfer coefficient, h, to represent the heat transfer through the walls. Obviously the value of h should account for several resistances including the thermal conductivity and thickness of the wall (which can consist of several layers with different conductivities and thicknesses) the heat transfer coefficient from the wall to the surrounding medium, which can be atmospheric air or a cooling fluid, for instance. Detailed models that take into account several of these features have been presented elsewhere.[6,8] Because in the present study the emphasis is to demonstrate the interconnection between microscale and macroscale phenomena that occur in the bed during the adsorption process, we preferred to simplify the heat transfer through the wall by considering overall "lumped" heat transfer coefficients instead of detailed heat balances for the walls and/or the cooling medium. The addition of such processes into the model is straightforward and the interested reader should consult the related references.

Initial Conditions ($t = 0$)

The bed is initially assumed to contain no hydrogen and to be at a constant temperature equal to the inlet temperature (although this is not necessary). In practice a small value for the initial pressure in the bed, P_0 is set for stability reasons ($P_0/P_f \approx 10^{-4}$–10^{-6}). This is totally justifiable from a practical perspective, too, because in reality no pump can produce an absolute vacuum inside the storage tank.

Solution of the model

The model of hydrogen storage by adsorption constitutes a set of integral, partial differential, and algebraic equations (IPDAEs). It is solved numerically using gPROMS,[30] a software package for the modeling and simulation of processes combining discrete and continuous characteristics. gPROMS allows the direct modeling of systems described by a combination of partial and/or ordinary differential equations combined if necessary with algebraic ones. The solution method is based on a two-phase method-of-lines approach. In the first phase the spatial dimensions (axial and radial) are discretized in terms of finite dimensional representations and this reduces the IPDAEs into sets of differential algebraic equations (DAEs). In the second phase the DAEs are integrated over the time horizon of interest using appropriate integration techniques. Here, the axial and radial domains are discretized using central finite differences with 20–30 points in each domain. Several simulations indicate that this number of points provides robust and accurate results without significant computational requirements. A typical simulation in gPROMS usually requires 1- to 2-min CPU time.

The most important parameter used to assess the performance of the storage process is the amount of hydrogen stored in the adsorbent m_t, defined as follows:

$$m_t = \frac{\int_{r=0}^{r=R} \int_{z=0}^{z=L} q(z, r) \cdot r dr dz}{\int_{r=0}^{r=R} \int_{z=0}^{z=L} r dr dz} \tag{17}$$

It is evident that parameter m_t has the same units as the concentration of H_2 in the adsorbed phase q (kg of H_2 per m^3 of adsorbent).

Determination of Optimal Sorption Properties from the Macroscopic Model

The process model (Eqs. 8–17) along with the boundary and initial conditions involve certain parameters characterizing the adsorbent material that must be optimally selected to achieve an economic and safe process performance. Such parameters are the macroscopic Langmuir constants q_s and b_0, whose values affect the maximum amount of hydrogen that can be stored in the bed for a specific charging time. There are two main issues that must be taken into consideration when estab-

lishing optimal control strategies for this system. The first is to ensure that the maximum process storage efficiency is achieved. The second is to ensure satisfaction of all operating and design constraints. This can be expressed by imposing an upper bound on the average bed temperature to account for potential safety concerns. The problem is posed as a dynamic optimization problem with the following general formulation:

$$\max_{q_s, b_0, \Delta H} (m_t)$$

Model equations (set of IPDAEs)

Boundary and initial conditions

$$\Delta T_{avg} \leq \Delta T_{bound}$$
$$q_s^{min} \leq q_s \leq q_s^{max}$$
$$b_0^{min} \leq b_0 \leq b_0^{max}$$

where ΔT_{bound}, q_s^{min}, q_s^{max}, b_0^{min}, and b_0^{max} are lower or upper bounds. The problem is solved using gPROMS dynamic optimization capabilities.[30]

Determination of Optimal Pore Size Distribution from the Microscopic Model

The problem of determining the pore size distribution of microporous carbons by combining molecular simulation and experimental isotherms of different probe molecules at room temperature has received considerable attention over the last decade.[31-37] The micropore range (from 0.6 to 2.0 nm) is subdivided in N equidistant intervals (classes of pores) with 0.1-nm spacing between them. The fraction of the total pore volume associated with each interval, is calculated on the basis of an assumed particle size distribution (PSD) and keeping the total pore volume equal to the measured one. Thus, the amount of gas adsorbed in every class at a certain pressure is evaluated by the simulation and, consequently, a computed isotherm is constructed. This, after comparison to its experimental counterpart, results in the optimum micropore size distribution provided by the best fit.

In the present study we have adopted the procedure defined above with one difference: The "experimental" isotherm that is used to derive the optimal pore size distribution is now obtained from the Langmuir equation where the parameters b_0 and q_s have been optimally determined from the macroscopic simulations described in the respective sections above.

The procedure for the determination of the optimum PSD involves the numerical solution of a minimization problem under certain constraints. In practice, the problem consists of minimizing the function

$$q_i - \sum_{j=1}^{N} d_{ij} w_j \qquad i = 1, M, j = 1, N \tag{18}$$

for M different pressure values P_i; where q_i (g/m^3) is the "experimentally" adsorbed amount determined at pressure P_i from the Langmuir isotherm (Eq. 12) with the optimally determined parameters b_0 and q_s. Variable d_{ij} is the calculated density of H_2 in a pore of width H_j at pressure P_i and w_j represents the fraction of pores with size H_j (as j changes from 1 to N, the whole micropore range from 0.6 to 2.0 nm is spanned with a step of 0.1 nm).

The elements of the vector of weight fractions **w** are subject to the constraints that they should be nonnegative and their sum should be equal to one:

$$w_j \geq 0 \qquad \sum_{j=1}^{N} w_j = 1 \qquad j = 1, N \tag{19}$$

The above problem can be reformulated to achieve better convergence as follows.

Because the sum of the weights is equal to one, we make the following substitution:

$$w_N = 1 - \sum_{j=1}^{N-1} w_j \tag{20}$$

Then the resulting minimization function and constraints become

$$(q_i - d_{iN}) - \sum_{j=1}^{N-1} (d_{ij} - d_{iN}) w_j \qquad i = 1, M, j = 1, N-1 \tag{21}$$

$$w_j \geq 0 \qquad \sum_{j=1}^{N-1} w_j \leq 1 \qquad j = 1, N-1 \tag{22}$$

A routine solving linearly constrained linear least-squares problems based on a two-phase (primal) quadratic programming method (E04NCF of NAG library) has been implemented. The routine has been successfully used in the past in studies involving experimental CO_2 sorption on carbons.[35,36]

It must be noted that the problem of determining the pore size distribution from a given isotherm is in general an ill-posed one. It is well known that the adsorption integral equation is a Fredholm linear equation of the first kind and the inversion of such equations results in ill-posed problems. Depending on the system, the minimization can lead to a multitude of solutions, so that several pore size distributions can produce the same known isotherm. Therefore, in all cases the issue of uniqueness of the solution vector **w** must be confirmed. In previously related studies,[32-37] several investigators including the present authors have applied numerical techniques that "artificially" overcome the inherent ill-posed character of the problem and ensure (to the best possible extent) the convergence to a stable solution. A detailed discussion of this issue, however, is clearly outside the scope of the present work. In particular, we have used in previous studies different N values (where N is the number of discrete pore sizes within the considered range, from 0.6 to 2.0 nm) and found that we obtain very similar solutions when N is such that the spacing between successive discrete pore sizes decreases to 0.1 nm. In the case presented in this manuscript, we have verified that the solutions obtained for the pore size distribution are indeed stable with

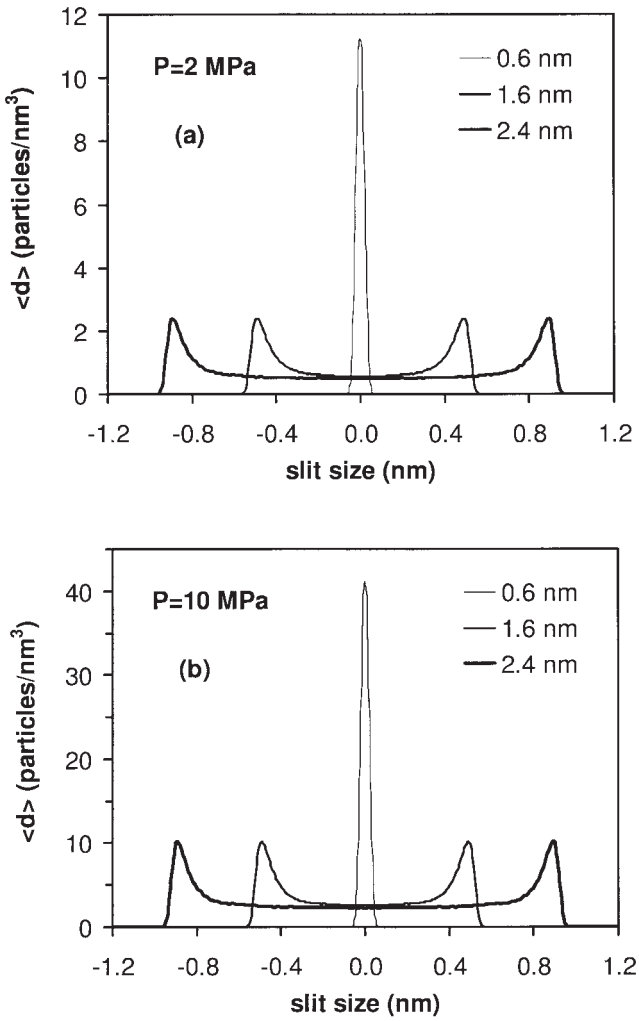

Figure 2. GCMC simulation results for the hydrogen density field, for three different pore sizes (T = 298 K).

respect to N regardless of the initial guess, pointing to the fact that our minimum is rather global than local. The produced isotherms are in all cases indistinguishable from the "optimal isotherm" found from the macroscopic study.

Results and Discussion

Iterative procedure

Molecular simulation results regarding hydrogen adsorption on different carbon slit sizes are shown in Figures 2 and 3. It is seen that strong confinement effects are present at small pore sizes (0.6 nm), resulting in close packing structures of the adsorbed hydrogen, which once formed, no longer change significantly with pressure. On the other hand, at large pore sizes (2.4 nm) there is significant space for the storage of hydrogen molecules, resulting in a continuous increase of sorption capacity as pressure increases further. However, even at pressures of 10 MPa, there is an abundance of empty space in the pore except from regions in the vicinity of the pore walls. Evidently, for pores of such sizes the effect of adsorption is masked by the effect of compression, particularly at high pressures. In fact, previous studies have shown that slit sizes $>$ 2.0 nm do not increase the excess adsorption in the pore. Therefore in the rest of the simulations we consider slit sizes between 0.6 and 2.0 nm.

Figure 4a depicts the hydrogen adsorption isotherms for different carbon slit sizes resulting from GCMC molecular simulations. It is seen that smaller pores (slits) adsorb larger amounts of hydrogen than larger pores on a per volume basis, whereas the reverse is true if we compare the amounts of hydrogen on a per mass basis.[10,11] In micropores the potentials exerted by the opposing pore walls are overlapping and thus deep potential energy wells are generated and, as a result, enhanced adsorption capacity is observed. Actually, the smaller the pore size, the deeper the potential well created and the stronger the interaction with adsorbate molecules (given that the pore is wide enough to be accessible by the adsorbate molecules). On the other hand, the pore volume is a linear function of pore width (in slit geometry) and thus smaller pores lead to smaller total amounts adsorbed at high pressures. Thus as we increase the pore size we increase the pore volume and accordingly we decrease the bulk density of the porous material. Detailed simulations at different slit sizes (every 0.1 nm) have shown the existence of a maximum adsorption capacity at a slit size of 0.7 nm.

This result might look contradictory at first glance because at pore widths of 0.7 nm only about one layer of H_2 molecules can adsorb, whereas pore sizes of about 1 nm can ensure a capacity of two layers and in general the molecular "packing" seems to be much more efficient inside larger pores. In this respect, when plotting the density of adsorbed phase vs. pressure for pores of different dimensions (such as 0.6 and 1.0 nm) it is always observed that at low pressures the density is higher in smaller pores. As the pressure is increased a crossing of the curves is observed and this leads to higher density in large pores at higher pressures. This is in accordance with the physics underlying adsorption in the sense that adsorbate molecules interact more strongly with the small pores (and thus more molecules are sorbed), but as the pressure is increased and the pores are progressively filled, blocking of the small pores occurs (that is, the density of the sorbed phase reaches a

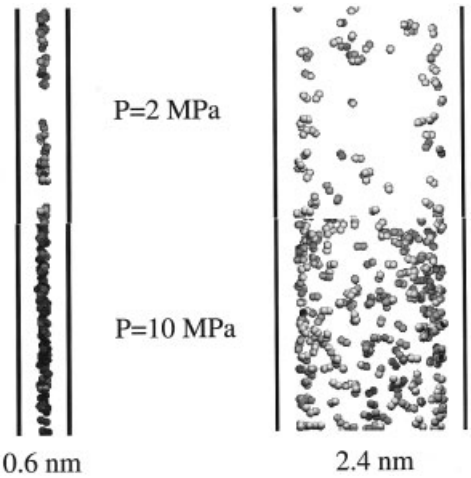

Figure 3. Visual representation of H_2 physisorption in the graphite nanopores (T = 298 K).

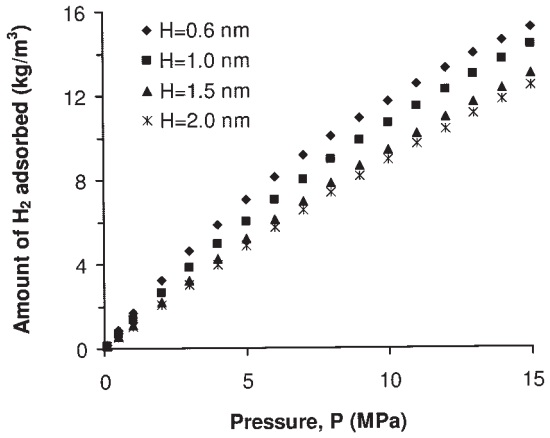

(a)

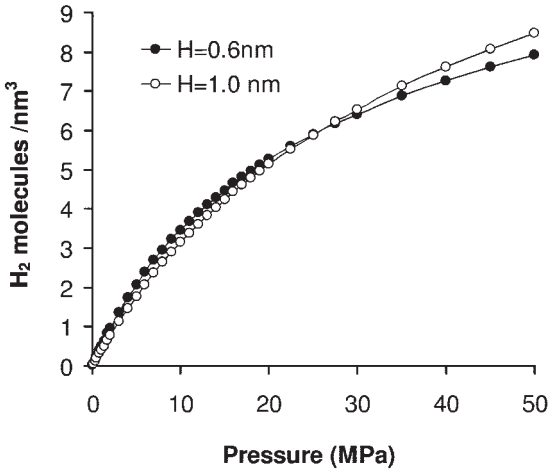

(b)

Figure 4. (a) Simulated H_2 adsorption isotherms for different pore sizes and pressures up to 15 MPa; (b) comparison of H_2 adsorption isotherms between pore sizes of 0.7 and 1.0 nm, for pressures up to 25 MPa (T = 298 K).

maximum value), whereas the molecules can still pack efficiently in larger pores. This is clearly depicted in Figure 4b, in which the density of sorbed H_2 (in molecules/nm^3) is plotted against the equilibrium H_2 pressure for two model pores (0.6 and 1.0 nm). The crossing of the two isotherms occurs at very high pressures (25 MPa), well beyond the practical limits of any H_2 storage process.

Based on the above we can safely conclude that at relatively low pressures (<25 MPa for the case of H_2 at 298 K) a single 0.6- to 0.7-nm pore is more efficient than a single 1-nm wide pore. Note that if we used a process temperature of 100 K we would have drawn completely different conclusions. In such a case the maximum packing of hydrogen is possible in the 1-nm pores at realistic pressures (3 MPa).[12] Detailed simulations on the effect of the operating temperature on the maximum carbon-based adsorbent performance can be found elsewhere.[12]

The amount predicted for the different pore sizes considered is in very good agreement with earlier studies using GCMC to calculate the adsorbed quantity of H_2 in carbon slit pores.[11] All isotherms fit very well to the Langmuir equation, enabling us to further use this equation in the macroscopic model.

From the microscopic simulations we have also computed the isosteric heat of adsorption for pore sizes between 0.6 and 2.0 nm. In Figure 5 we show the effect of the pore size on the isosteric heat of adsorption, $|\Delta H|$. It is seen that $|\Delta H|$ has its maximum value, about 10 kJ/mol, at $H = 0.6$ nm, and exhibits a steep monotonic decrease to nearly 5 kJ/mol up to $H = 1$ nm, and a smoother decrease to 4.4 kJ/mol as we approach $H = 2$ nm. Thus, $|\Delta H|$ is a strong function of the pore size, particularly for pores with size < 1 nm.

From the results of the microscopic simulation it is evident that there is a two-way interaction between the macroscopic and the microscopic models. More specifically, the macroscopic model determines the optimum isotherm parameters that should be used further in the microscopic model to obtain the optimum pore size distribution of the material. On the other hand, both the heat of adsorption $|\Delta H|$ and the bulk density of the material ρ_s—input parameters in the macroscopic model—depend on the pore size distribution, which is obtained by the microscopic model. It is therefore clear that the macroscopic model depends on the results of the microscopic model, and particularly on the pore size distribution, which determines the values of ΔH and ρ_s. Therefore the following iterative process is used:

(1) From the macroscopic model the optimum sorption isotherm parameters are determined, given initial guess of the heat of adsorption $|\Delta H^{(0)}|$ and bulk density of the material $\rho_s^{(0)}$.

(2) From the microscopic model the optimum pore size distribution is determined corresponding to the Langmuir isotherm data, based on the above parameters.

(3) From the optimum pore size distribution the "new" values of $|\Delta H|$ and ρ_s are computed.

(4) Steps 1–3 are repeated until convergence is achieved.

The above iterative procedure is used for different temperature constraints, ΔT_b. Note that the constraints are imposed on the average bed temperature rise because a faster and more stable convergence of the dynamic optimization algorithm is achieved, as opposed to the case when the maximum temperature is constrained.[8] It must be noted that ΔH computed in step 3 is found to change slightly with coverage and for this reason an average value of this parameter is calculated and becomes

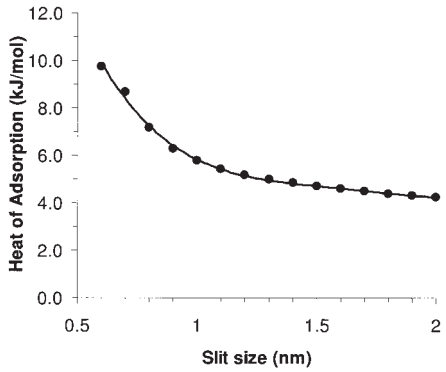

Figure 5. Simulated heats of adsorption for different pore sizes (T = 298 K).

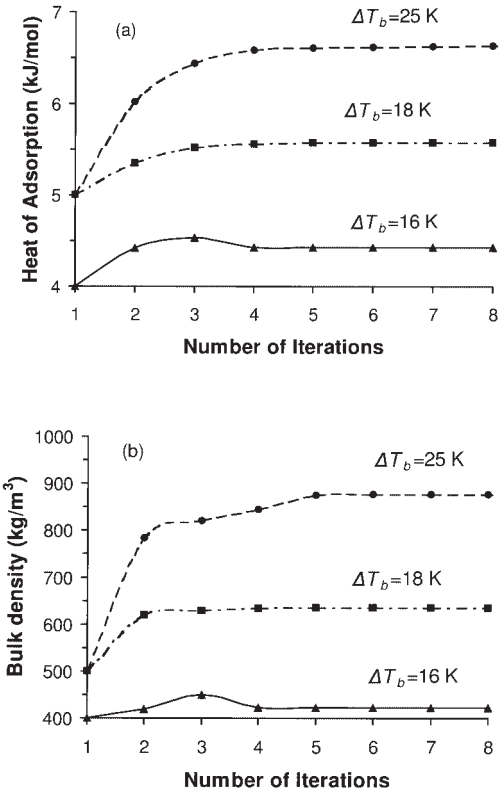

Figure 6. Convergence of the heat of adsorption and the bulk density of the material through the multiscale iterative procedure.

an input in the macroscopic model (step 1). This simplification is in full accordance with previous macroscopic modeling studies.[5,6]

Typical results from the iterative process are shown in Figure 6. It is seen that after four to five iterations no significant change is observed in the values of ΔH and ρ_s and essentially the iterative procedure has converged. The same is true for the values of the optimized Langmuir parameters, q_s and b_0, and for the resulting pore size distribution as seen in Figure 7.

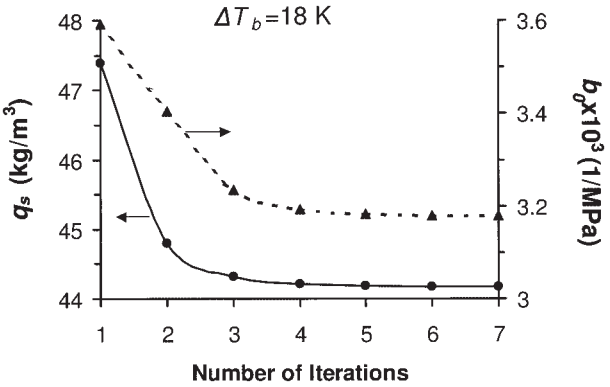

Figure 7. Convergence of the Langmuir parameters through the multiscale iterative procedure.

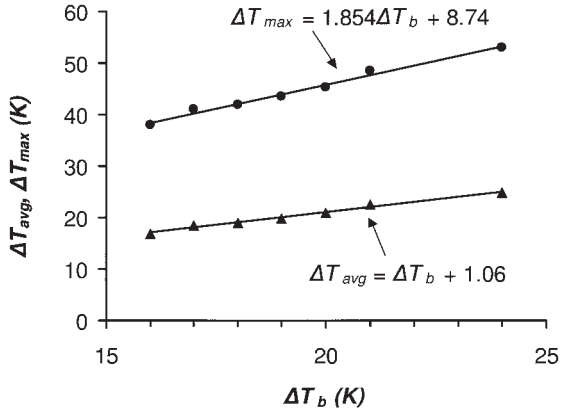

Figure 8. Effect of the imposed temperature bounds on the average and maximum temperature rise in the storage tank.

Effect of the temperature constraints

In Figure 8, we present the relation between the imposed temperature constraint (ΔT_b) and the resulting maximum ($\Delta T_{\max}$) and maximum-average temperature (ΔT_{avg}), appearing in the bed, for a storage time of 400 s. We observe that both ΔT_{avg} and $\Delta T_{\max}$ increase linearly with ΔT_b. ΔT_{avg} differs from ΔT_b by 1 K, which is consistent with the tolerances imposed in the optimization process, whereas $\Delta T_{\max}$ is more than twice ΔT_{avg} in all cases.

Figure 9 presents the resulting values of the bulk density and heat of adsorption of the optimized material for different temperature constraints. It is seen that as we relax the temperature constraints (that is, increase ΔT_b) we obtain optimized materials with higher bulk density and heat of adsorption. This is expected because both values contribute to the heat release and thus to the temperature rise in the storage tank.

Figure 10 illustrates the resulting densities of H_2 stored in the carbon-based optimized materials on a per volume and per weight basis. It is interesting to observe that the two densities show a completely opposite trend as the temperature constraint changes. In particular, as ΔT_b decreases so does the volumetric density of H_2, whereas its gravimetric density increases. The apparent contradiction is easily explained, given that as ΔT_b decreases so does the density of the optimized material, as

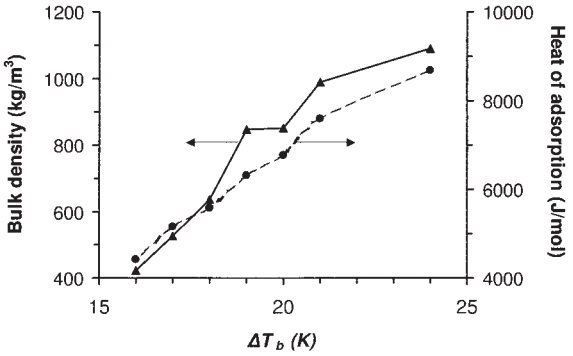

Figure 9. Effect of the imposed temperature bounds on the converged value of the heat of adsorption and the bulk density of the material.

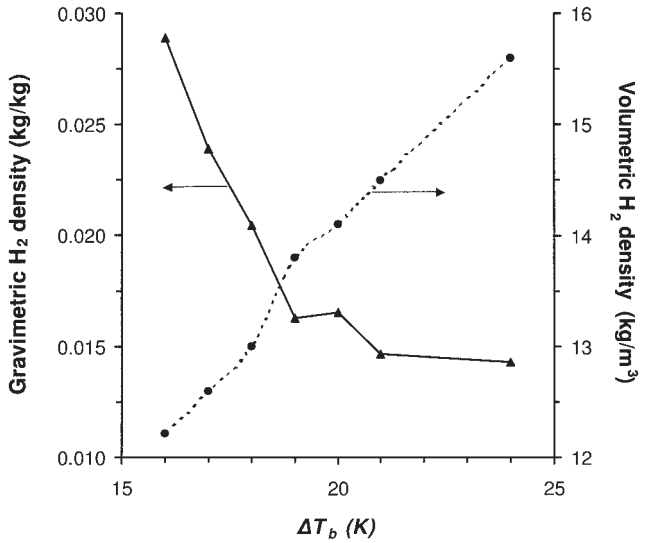

Figure 10. Effect of the imposed temperature bounds on the optimum value of the gravimetric and volumetric hydrogen density stored in the adsorbent.

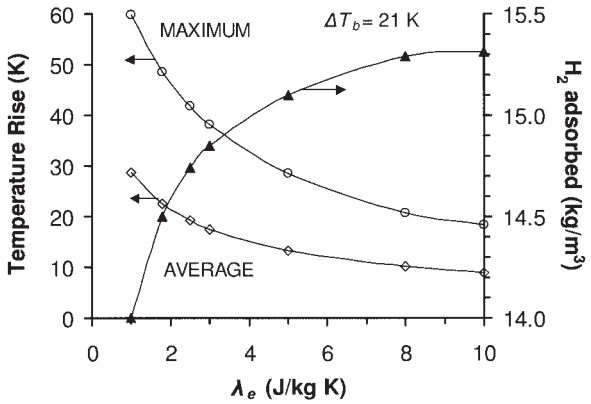

Figure 12. Effect of the thermal conductivity of the storage tank on the process performance for an optimized adsorbent at a temperature bound (ΔT_b) of 21 K.

already seen in Figure 9. Thus, when evaluating the performance of the material it is important to consider its density together with the maximum amount of H_2 adsorbed if the comparison is on a per weight basis or, alternatively, the comparison should be done on a per volume basis.

The optimal pore size distributions that result from the optimization procedure are depicted in Figure 11. It is evident that when loose bounds are imposed on the temperature rise in the bed (high ΔT_b), the optimum pore size distribution is very narrow and it is limited to sizes of $\leq$1 nm (where the amount of adsorbed H_2 is maximum). On the other hand, as the temperature bounds are tightened, we observe a shift of a fraction of pores toward larger sizes, where both the volumetric hydrogen density and the heat of adsorption of the material are significantly lower, as can be seen from Figure 4. This shifting results in a decrease in the bulk density of the material and thus in a reduction of the volumetric density of H_2 stored in the adsorbent.

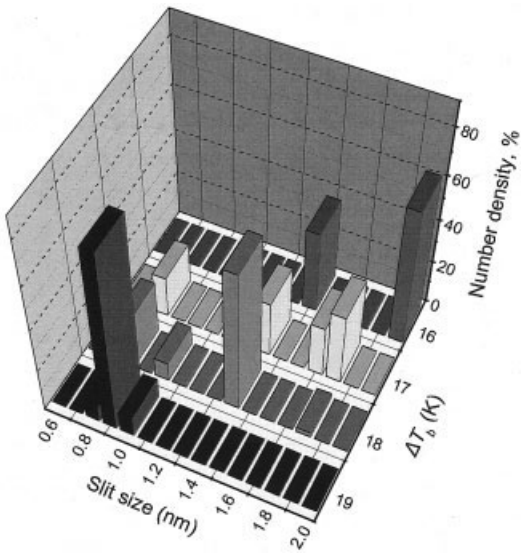

Figure 11. Effect of the imposed temperature bounds on the optimal pore distributions of the adsorbent.

To elaborate more on the optimal PSD results shown in Figure 11, we must note that the total pore volume is determined every time from the macroscopic "optimal" isotherm and remains unchanged in the course of a single minimization run that is used to determine the optimal PSD. Thus the optimization code can add "more" small pores or "fewer" larger ones to fill up the predetermined total pore volume. In this respect the use of small pores adding up to a certain total pore volume is much more efficient than using larger ones adding to the same total pore volume. This is based on the fact that the surface area of the material is dramatically increased, whereas adsorption is further enhanced as a result of the deeper potential wells (this holds for the relatively low pressures of $\leq$15 MPa considered in storage processes). On the other hand, as the pores become very narrow and thus surface area is increased, whereas the interactions are stronger the heat of adsorption is rapidly increasing, so the quantity of heat exchanged becomes larger and this is why pore size distributions containing primarily small pores are efficient only when a loose temperature difference constriction is imposed.

Effect of the heat conduction coefficient

It was found before that increasing the effective thermal conductivity of the material λ_e and, even more important, the conductivity in the radial direction results in a significant decrease of the generated temperature rise in the storage tank.[5,6] Thus we varied this parameter up to about ten times to study the effect of λ_e on the process performance. Note that such an increase in λ_e is feasible through a process that involves mechanical consolidation of the grains of activated carbon and subsequent mixing with expanded natural graphite.[38,39] The results are presented in Figure 12 for ΔT_b = 21 K. As expected, one can decrease the maximum temperature rise

in the bed by as much as 40 K and thus increase the volumetric density of hydrogen by 11%.

Effect of the storage time

We varied the storage time from 300 to 600 s to study its effect on the process performance. The results are presented in Figure 13 for $\Delta T_b = 21$ K. As expected, increasing the storage time results in an improvement in the performance of the storage process. However, it is important to emphasize that the value of this parameter is typically controlled by practical considerations because the charging time must be quite short, especially when mobile applications[6] are considered.

Adsorbent evaluation

The usable capacity ratio (UCR), one of the criteria used to judge the performance of an adsorbent,[40] is defined as the ratio of the mass of available hydrogen in a tank packed with the adsorbent over the mass of available hydrogen in an empty tank of the same dimensions (compressed gas only). Note that in this calculation one should take into account the porosity of the storage tank. The term "available" denotes the difference between the amount of hydrogen at the storage pressure and the amount of hydrogen at the discharge pressure (normally atmospheric). Thus, the UCR is essentially a measure of the effectiveness of sorption compared to gas compression at the same temperature and pressure conditions. If UCR $>$ 1 then the sorption process is more effective, whereas if UCR $<$ 1 then compression prevails. In Figure 14 we present the UCR values at $P = 15$ MPa and $T = 298$ K for the different temperature bounds imposed in the optimization process. It is seen that as we tighten the temperature bounds the value of UCR decreases. At the maximum value of ΔT_b imposed, $\Delta T_b = 24$ K, UCR = 1.16, which means that we have a 16% increase in the adsorption process efficiency compared to gas compression. On the other hand, at the minimum value of ΔT_b imposed, $\Delta T_b = 16$ K, UCR = 1.02, which means only a 2% increase in the process efficiency. Obviously, however, there are several additional parameters that must be considered before a proper evaluation of the material is attempted; based on these preliminary results it seems that we cannot achieve reasonably high UCR values for pore size distributions that satisfy too strict temperature constraints ($\Delta T_b < 20$ K). Thus if we want to achieve lower temperature rises in the bed, we must increase the effective thermal conduction coefficient of the adsorbent.

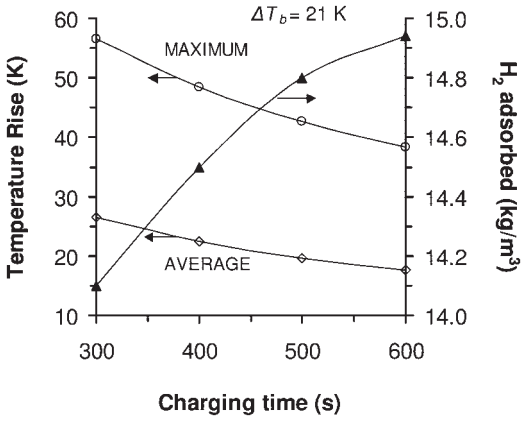

Figure 13. Effect of the charging time on the process performance for an optimized adsorbent at a temperature bound (ΔT_b) of 21 K, for a linear profile of the inlet pressure with time.

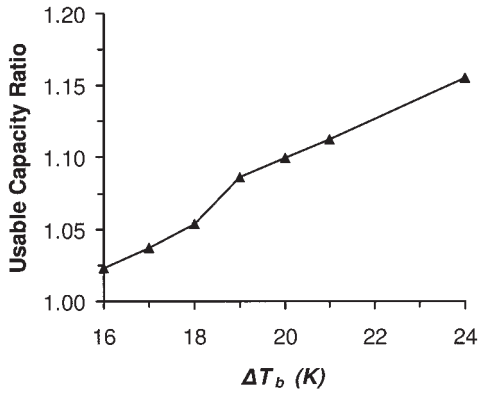

Figure 14. Effect of the imposed temperature bounds on the usable capacity ratio (UCR) of the optimized adsorbent.

Conclusions

The present work presents a multiscale modeling and optimization framework for hydrogen storage in carbon-based materials. The outlined methodology is generic and can be easily adapted to the storage of several gases of relevant importance [such as methane,[39,41] carbon dioxide,[35] and/or different nanoporous adsorbents (metal-doped carbon nanotubes,[42] zeolites,[43,44] metal–organic frameworks,[45-47] etc.)].

The results clearly indicate how realistic operating constraints (such as temperature limitations arising from safety considerations) can affect the material design and how material design constraints (such as those arising from manufacturing limitations) can effect the operation and efficiency of the process. More particularly, when loose temperature bounds are imposed, the optimum pore size distribution is very narrow, limited in sizes of $\leq$1 nm, where the amount of adsorbed H_2 is maximum. On the other hand, as the temperature bounds are tightened, a shifting of a fraction of pores toward larger sizes is observed, resulting is significantly lower values of both the volumetric hydrogen density and the heat of adsorption of the material. Furthermore, the performance of the storage process can be significantly increased, as expected, when increasing the thermal conductivity of the adsorbent and the storage time for a linear profile of the inlet pressure with time.

Current work focuses on exploring further optimization opportunities in the process (such as by optimizing the inlet pressure charging history or by incorporating detailed CFD simulations for the cooling system) and their effect on material design. A more comprehensive macroscopic model including an integrated heat exchange system is also under development. The ultimate objective is to systematically reveal the strong and highly related synergistic benefits between process design/operation decisions and material design aspects so as to ensure an economically attractive, technically feasible, and safe process.

Acknowledgments

The authors gratefully acknowledge the partial financial support from the European Commission DG Research (Contract: SES6-2004-502667/STORHY).

Notation

a = parameter controlling the rate of pressure charging
b_0 = Langmuir parameter defined in Eq. 12
C_{pg} = heat capacity of the gas
C_{ps} = heat capacity of the adsorbent
h = overall heat transfer coefficient
H = slit-pore width
H' = corrected pore width
$\mathbf{K}$ = permeability tensor
k = mass transfer coefficient
L = total bed length
m_t = total amount of hydrogen stored in the tank
P = pressure in the bed
P_f = pressure at the bed inlet
q = hydrogen amount adsorbed
q^* = hydrogen amount adsorbed
q_s = saturation amount adsorbed according to the Langmuir isotherm, Eq. 12
R = total bed radius
r = radial distance
t = time
t_c = charging time
t_s = storage time
T_f = temperature at the bed inlet
$\mathbf{u}$ = superficial gas velocity vector
z = axial distance

Greek letters

Δ = distance between the stack layers in the carbon nanopore
$(-\Delta H)$ = heat of adsorption
ε = bed porosity
ε_{HH} = well depth energy
λ_e = effective thermal conductivity
ρ = hydrogen density in the gas phase
ρ_f = hydrogen density at the bend inlet
ρ_s = solid density of the adsorbent
ρ_w = number density of carbon atoms at the pore wall
σ_{HH} = Lennard–Jones hard-sphere diameter for H atoms

Literature Cited

1. Mohanty KK. The near-term energy challenge. *AIChE J.* 2003;49:2454–2460.
2. Agrawal R, Offutt M, Ramage MP. Hydrogen economy—An opportunity for chemical engineers. *AIChE J.* 2005;51:1582–1589.
3. Momirlan M, Veziroglu TN. Current status of hydrogen energy. *Renew Sustain Energy Rev.* 2002;6:141–179.
4. Jemni A, Nasrallah SB. Study of two-dimensional heat and mass transfer during absorption in a metal-hydrogen reactor. *Int J Hydrogen Energy.* 1995;20:1:43–52.
5. Lamari M, Aoufi A, Malbrunot P. Thermal effects in dynamic storage of hydrogen by adsorption. *AIChE J.* 2000;46:632–646.
6. Delahaye A, Aoufi A, Gicquel A, Pentchev I. Improvement of hydrogen storage by adsorption using 2-D modelling of heat effects. *AIChE J.* 2002;48:2061–2073.
7. Aldas, K. Mat MD, Kaplan Y. A three-dimensional model for absorption in a metal hydride bed. *Int J Hydrogen Energy.* 2002;27:1049–1056.
8. Kikkinides ES, Georgiadis MC, Stubos AK. On the optimisation of hydrogen storage in metal hydride beds. *Int J Hydrogen Energy.* 2006;31:737–751.
9. Darkrim F, Levesque D. Monte Carlo simulations of hydrogen adsorption on single-walled carbon nanotubes. *J Chem Phys.* 1998;109:4981–4984.
10. Wang Q, Johnson JK. Computer simulations of hydrogen storage on graphitic nanofibers. *J Phys Chem.* 1999;103:277–281.
11. Cracknell RF. Molecular simulation of hydrogen adsorption in graphic nanofibres. *Phys Chem Chem Phys.* 2001;3:2091–2097.
12. Bhatia SK, Myers AL. Optimum conditions for adsorptive storage. *Langmuir.* 2006;22:1688–1700.
13. Gerogiorgis DI. *Multiscale CFD Modeling for Design, Simulation and Stability of Distributed Chemical Process Systems: Application to Carbothermic Aluminum Production*. PhD Dissertation. Pittsburgh, PA: Carnegie Mellon University; 2004.
14. Pantelides CC. New challenges and opportunities for process modeling. In Jørgensen SB, Gani R, eds. *Proceedings of the European Symposium on Computer Aided Process Engineering (ESCAPE–11)*. Amsterdam, The Netherlands: Elsevier; 2001:15-26.
15. Nicholson D, Parsonage NG. *Computer Simulations and the Statistical Mechanics of Adsorption*. New York, NY: Academic Press; 2001.
16. Allen M, Tildesley DJ. *Computer Simulation of Liquids*. Oxford, UK: Clarendon; 1987.
17. Steele WA. *The Interaction of Gases with Solid Surfaces*. Oxford, UK: Pergamon; 1974.
18. Nicholson D. Simulation study of nitrogen adsorption in parallel-sided micropores with corrugated potential functions. *J Chem Soc Faraday Trans.* 1994;90:181–185.
19. Levesque D, Gicquel A, Lamari Darkrim F, Beyaz Kayiran S. Monte Carlo simulations of hydrogen storage in carbon nanotubes. *J Phys Condens Matter.* 2002;14:9285–9293.
20. Feynman RP. Space-time approach to non-relativistic quantum mechanics. *Rev Mod Phys.* 1948;20:367–387.
21. Feynman RP, Hibbs AR. *Quantum Mechanics and Path Integrals*. New York, NY: McGraw-Hill; 1965.
22. Wang Q, Johnson JK, Broughton JQ. Path integral grand canonical Monte Carlo. *J Chem Phys.* 1997;107:5108–5117.
23. Yin YF, Mays TJ, McEnaney B. Adsorption potentials and simulations in carbon slits and cylinders. In Meunier F, ed. *Proceedings of the Sixth International Conference on Fundamentals of Adsorption FOA6, Gien, France, May 24–26, 1998*. Amsterdam, The Netherlands: Elsevier; 1998:261-266.
24. Ruthven DM. *Principles of Adsorption and Adsorption Processes*. New York, NY: Wiley; 1985.
25. Yang RT. *Gas Separation by Adsorption Processes*. Boston, MA: Butterworths; 1987.
26. Glueckauf E. Theory of chromatography, Part II. Formulae for diffusion into spheres and their application to chromatography. *Trans Faraday Soc.* 1955;51:1540–1551.
27. Liaw CM, Wang JSP, Greenkorn RA, Chao KC. Kinetics of fixed bed adsorption: A new solution. *AIChE J.* 1979;25:376–381.
28. Do DD, Rice RG. Validity of the parabolic profile assumption in adsorption studies. *AIChE J.* 1986;32:149–154.
29. Nicholson D. A simulation study of energetic and structural heterogeneity in slit-shaped pores. *Langmuir.* 1999;15:2508–2515.
30. Process Systems Enterprise Ltd. *gPROMS Advanced Users Guide*. London, UK; 2004.
31. Lastoskie C, Gubbins KE, Quirke N. Pore-size distribution analysis of microporous carbons—A density-functional theory approach. *J Phys Chem.* 1993;97:4786–4796.
32. Gusev VI, O'Brien JA, Seaton NA. A self-consistent method for characterization of activated carbons using supercritical adsorption and Grand Canonical Monte Carlo simulations. *Langmuir.* 1997;13:2815–2821.
33. Davies GM, Seaton NA, Vassiliadis VS. Calculation of pore size distributions of activated carbons from adsorption isotherms. *Langmuir.* 1999;15:8235–8245.
34. Ravikovitch PI, Vishnyakov A, Russo R, Neimark AV. Unified approach to pore size characterization of microporous carbonaceous materials from N_2, Ar and CO_2 adsorption isotherms. *Langmuir.* 2000;16:2311–2320.
35. Samios S, Stubos A, Papadopoulos GK, Kanellopoulos NK, Rigas F. The structure of adsorbed CO_2 in slitlike micropores at low and high temperature and the resulting micropore size distribution based on GCMC simulations. *J Colloid Interface Sci.* 2000;224:272–290.
36. Samios S, Papadopoulos G, Steriotis TA, Stubos AK. Simulation study of sorption of CO_2 and N_2 with application to the characterization of carbon adsorbents. *Mol Simul.* 2001;27:441-456.

37. Sweatman MB, Quirke N. Characterization of porous materials by gas adsorption at ambient temperatures and high pressure. *J Phys Chem B*. 2001;105:1403–1411.
38. Olives R, Mauran S. A highly conductive porous medium for solid–gas reactions: Effect of dispersed phase on the thermal tortuosity. *Transp Porous Media.* 2001;43:377–394.
39. Biloe S, Goetz V, Mauran S. Dynamic discharge and performance of a new adsorbent for natural gas storage. *AIChE J*. 2001;47: 2819–2830.
40. Benard P, Chahine R. Modeling of adsorption storage of hydrogen on activated carbons. *Int J Hydrogen Energy.* 2001;26:849–855.
41. Mota JPB, Rodrigues AE, Saatdjian E, Tondeur D. Dynamics of natural gas adsorption storage systems employing activated carbon. *Carbon.* 1997;35:1259–1270.
42. Lueking A, Yang RT. Hydrogen storage in carbon nanotubes: Residual metal content and pretreatment temperature. *AIChE J.* 2003;49:1556–1568.
43. Nijkamp MG, Raaymakers JEMJ, van Dillen AJ, de Jong KP. Hydrogen storage using physisorption—Materials demands. *Appl Phys A.* 2001;72:619–623.
44. Langmi HW, Walton A, Al-Mamouri MM, Johnson SR, Book D, Speight JD, Edwards PP, Gameson I, Anderson PA, Harris IR. Hydrogen adsorption in zeolites A, X, Y and RHO. *J Alloys Comp.* 2003;356:710–715.
45. Li H, Eddaouddi M, O'Keeffe M, Yaghi OM. Design and synthesis of an exceptionally stable and highly porous metal-organic framework. *Nature.* 1999;402:276–279.
46. Rowsell JLC, Millward AR, Park KS, Yaghi OM. Hydrogen sorption in functionalized metal-organic frameworks. *J Am Chem Soc.* 2004; 126:5666–5667.
47. Panella B, Hirscher M. Hydrogen physisorption in metal-organic porous crystals. *Adv Mater.* 2005;17:538.

Manuscript received Dec. 1, 2005, and revision received May 4, 2006.